Trajectory Tracking Control for Disturbed Euler-Lagrange Systems: A Fixed-Time Adaptive Approach

Zeeshan Anjum*,*, Zhe Sun**, Hazrat Bilal***, Khubab Ahmed****

**School of Mechanical and Electrical Engineering, Quanzhou University of Information Engineering, Quanzhou 362000, China;*
***College of Information Engineering, Zhejiang University of Technology, Hangzhou 310023, China; (e-mail:zeeshananjum139@outlook.com, sunzhe726@zjut.edu.cn, khubab@hotmail.com).*
****College of Mechatronics and Control Engineering, Shenzhen University, Shenzhen 518000, China (e-mail:hbilal@mail.ustc.edu.cn).*
Corresponding author: Zeeshan Anjum and Zhe Sun

Abstract: This paper primarily focuses on addressing the challenging problem of trajectory tracking control for a specific class of Euler-Lagrange systems subjected to uncertainties and disturbances. A fixed-time tracking control strategy based on sliding mode is introduced, featuring a modified fixed-time sliding mode variable that exhibits shorter convergence time compared to conventional fixed-time sliding variable. This sliding mode variable has no singularity and can guarantee the settling-time to be independent of initial states. Furthermore, attaining the upper bound presents challenges given the uncertainty surrounding the disturbance. Consequently, an adaptation mechanism is incorporated into fixed-time nonsingular sliding mode (FTNSM) to devise a continuous adaptive FTNSM control law. This method entails estimating the disturbance upper bound using adaptive techniques, thus obviating the requirement for prior knowledge and efficiently alleviating the disturbance's influence on the system while also potentially mitigating the chattering phenomenon. Lyapunov theory shows that the closed-loop tracking system is stable and converges in a fixed amount of time. Theoretical analysis demonstrates that the proposed sliding mode variable, along with the errors, can converge within narrow vicinity within the specified time frame. Numerical simulations illustrate that despite uncertainties and disturbances, the proposed controller effectively achieves trajectory tracking with high accuracy and stability.

Keywords: Euler-Lagrange (EL) systems, sliding mode control, fixed-time stable, tracking control, uncertainty

1. INTRODUCTION

As commonly understood, Euler-Lagrange (EL) systems can effectively represent various practical systems including robotic systems, quad rotor aircraft, spacecraft and tethered satellite systems. The operational behavior of these systems is profoundly influenced by both their operational environment and the materials utilized in their construction, a fact supported by reference (Saeed et al., 2020). Additionally, these systems consistently face a myriad of challenges, ranging from external disruptions to uncertainties in modeling, nonlinear dynamics, and delays. Consequently, the control problem pertaining to EL systems has garnered significant attention over recent decades. Extensive research has yielded numerous insights into stability and tracking methodologies for physical systems, highlighting sliding-mode control (SMC) (Wang et al., 2021), model predictive control (Sun et al., 2017), adaptive control (Jin et al., 2017), observer-based control (Deng et al., 2021), intelligent control (Qin et al., 2014), and other advanced control techniques as the most promising solutions. The SMC method, belonging to the variable structure control family, adapts the control law structure to the evolving system dynamics over time, as extensively discussed in (Shtessel et al., 2014). Hence, SMC stands out as a prominent approach for mitigating system imperfections. Recently, in (Ren et al., 2019), a specific SMC law was proposed for EL systems, ensuring asymptotic convergence of trajectory tracking errors. However, linear SMC only guarantees asymptotic convergence of system states, without determining the convergence time. To achieve faster convergence rates, terminal SMC techniques were introduced in (Venkataraman and Gulati, 1993), aiming to ensure system state convergence within finite time. Nevertheless, terminal SMC introduces singularity issues due to fractional powers, prompting the development of nonsingular terminal SMC methods in (Feng et al., 2002) to circumvent this problem. Additionally, an indirect approach was devised in (Wang et al., 2009) to transform the terminal sliding surface into a linear one, thereby eliminating singular values. Nevertheless, in the utilization of the previously mentioned terminal SMC or nonsingular terminal SMC control algorithms, if initial information is inaccessible, the settling time cannot be predetermined, leading to the absence of explicit estimates for the reaching time.

In order to achieve a desired settling time, the concept of fixed-time stability was introduced in (Polyakov, 2011). Unlike finite-time techniques, the fixed-time approach demonstrates improved convergence performance even when initial system states are unknown (Zuo, 2015). Fixed-time stability represents a further advancement from finite-time stability in terminal SMC (TSMC), achieved by substituting the power-one term of the fast terminal sliding manifold with a power-greater-than-one term, thereby ensuring an upper bound settling time regardless of initial states. In (Huang and Jia, 2018), an adaptive controller was developed for noncooperative spacecraft by integrating the designed fixed-time TSMC technique with adaptive methods, aiming to attain fixed-time reachability. Building upon the fixed-time technique and backstepping technique, (Song et al., 2020) introduced an adaptive fuzzy controller to guide unmanned surface vehicles in tracking desired trajectories within predefined timeframes.

Over the recent years, the fixed-time control methodology has been increasingly utilized to address control challenges in EL systems. In pursuit of fixed-time attitude stabilization for spacecraft, (Gao et al., 2018) explored a fixed-time control technique based on integral fixed-time sliding mode and observer mechanisms. Additionally, (Zhang et al., 2021) proposed an adaptive fault-tolerant control scheme incorporating fixed-time terminal sliding mode control for uncertain robotic manipulator systems. Despite its advantage in enhancing convergence rates, the fixed-time algorithm may encounter singularity issues akin to finite-time TSMC. Addressing this concern, (Jiang et al., 2016) presented a fixed-time control approach for stabilizing the attitude of rigid spacecraft with actuator faults and input saturation, although the inclusion of the signum function in the control law could lead to undesirable chattering. In (Cao et al., 2019), a singular-free fixed-time sliding mode was developed by implementing an indirect switching approach near the singular value.

While existing control schemes have generally achieved satisfactory tracking performance, only a limited number of studies have specifically focused on improving transient response. In (Fallaha et al., 2010), a control scheme based on an exponential reaching law was proposed for robotic systems, aiming to reduce reaching time during transient states. Subsequently, (Mozayan et al., 2016) introduced an enhanced exponential reaching law to further refine transient response, although chattering issue persisted in steady states. Building upon these findings, (Chen et al., 2018) presented an attitude control method for rigid spacecraft to expedite reaching time and enhance convergence speed of the sliding mode surface. In (Tao et al., 2019), a novel double power reaching law was developed using an inverse trigonometric function, intending to accelerate state stabilization and concurrently reduce chattering phenomenon.

Consequently, ensuring rapid convergence in transient state while mitigating chattering in steady state poses a challenging task.

Building on the preceding discourse, this study introduces a trajectory tracking control approach tailored for a specific subset of EL systems characterized by reduced chattering and fast fixed-time convergence. The principal advancements presented in this paper include:

1. A fast FTNSM variable devoid of singularity is devised to achieve swifter convergence rate compared to the FTNSM variables referenced in literature (Huang and Jia, 2017; Ni et al., 2016).

2. In managing EL systems, the existence of inherent uncertainty and external disturbances presents tangible hurdles. The effective consideration of these factors holds paramount importance in ensuring the robust performance of control systems. To bolster the control system's resilience against uncertainties and disturbances, an adaptation law is integrated into the FTNSM. This integration equips the adaptive FTNSM control law to adeptly address the effects of uncertainties and disturbances encountered in real-world scenarios.

3. Thorough theoretical demonstrations indicate that the proposed adaptive FTNSM control law exhibits several advantageous attributes, including fixed-time convergence within confined regions, rapid convergence, mitigation of chattering, and independence from prior knowledge of disturbance upper bounds.

The remainder of this paper is organized as follows: The next section presents the necessary background information and defines the problem. Section 3 displays the principal findings, emphasizing an adaptive FTNSM control system for EL systems that achieves highly accurate trajectory tracking within a predetermined time frame. Section 4 includes the presentation of verification through simulation experiments. Finally, Section 5 offers the conclusion.

2. PROBLEM FORMULATION AND MATHEMATICAL PRELIMINARIES

Notations. Regarding a specific vector $\mathbf{y} = \left[y_1, y_2, ..., y_n\right]^{\mathrm{T}}$, $\mathbf{sig}(\mathbf{y})^a = \left[\mathrm{sig}^a(y_1), \mathrm{sig}^a(y_2), ...\mathrm{sig}^a(y_n)\right]^{\mathrm{T}}$, where $\mathrm{sig}^a(y_i) = |y_i|^a \,\mathrm{sign}(y_i), i = 1,2,3,...,n$. with $\mathrm{sign}(.)$ denotes the sign function and $a \in \Re$ is a constant . The symbol $|\bullet|$ is the absolute value of a scalar and $\|\bullet\|$ denotes the Euclidean norm of a matrix or a vector.

2.1 Mathematical preliminaries

Consider the following system

$$\dot{y} = f\left(y(t)\right), y(0) = y_0, f(0) = 0 \tag{1}$$

where $y \in \Re^n$ and $f : \Re^n \to \Re^n$ is a nonlinear function.

Definition 1. (Tian et al., 2017) System (1) is classified as fixed-time stable when it exhibits global finite-time stability. Consequently, it will reach the origin within a bounded convergence time $T(y_0)$. In this context, there exists a positive constant $T_{\max}$ such $T(y_0) < T_{\max}$.

Lemma 1. (Polyakov, 2011; Rezaei et al., 2024) Suppose there exists a continuously differentiable Lyapunov function $V(y)$ for system (1), satisfying the inequality:

$$\dot{V}(y) \le -\alpha_1 V(y)^{q_1} - \beta_1 V(y)^{q_2} + \upsilon_t, \tag{2}$$

where $\alpha_1, \beta_1 \in \Re^+, 0 < q_1 < 1, q_2 > 1$ and $\upsilon_t \in \Re^+$. Under these conditions, the system is practically fixed-time stable. This means that the system can be stabilized within a fixed-time to a residual set R_t that includes the equilibrium point. The residual set is defined as:

$$R_t = \left\{ y \,|\, V(y) \le \min\left\{ \left(\frac{\upsilon_t}{((1-\upsilon_\theta)\alpha_1)} \right)^{1/q_1}, \left(\frac{\upsilon_t}{((1-\upsilon_\theta)\beta_1)} \right)^{1/q_2} \right\} \right\} \tag{3}$$

where $0 < \upsilon_\theta < 1$. Furthermore, the upper bound on the convergence time is given by:

$$T(y_0) \le \frac{1}{\alpha_1(1-q_1)} + \frac{1}{\beta_1(q_2-1)}, \forall y_0 \in \Re^n. \tag{4}$$

Lemma 2. (Zuo et al., 2017) Let $y_i \in \Re$ for $i = 1, 2, 3, ..., n$, and let $0 < v \le 1$. Under these conditions, the following inequality holds:

$$\sum_{i=1}^{n} |y_i|^v \ge \left(\sum_{i=1}^{n} |y_i| \right)^v \tag{5}$$

Lemma 3. (Zuo et al., 2017) Let $y_i \in \Re$ for $i = 1, 2, 3, ..., n$, and let $v_1 > 1$. Then, the following inequality holds:

$$\sum_{i=1}^{n} |y_i|^{v_1} \ge n^{1-v_1} \left(\sum_{i=1}^{n} |y_i| \right)^{v_1} \tag{6}$$

2.2 Euler-Lagrange systems

Take into account the dynamics of the EL system as presented in reference (Spong and Vidyasagar, 2008).

$$\ddot{\mathbf{q}}_t = \mathbf{M}^{-1}(\mathbf{q}_t)(\boldsymbol{\tau} - \mathbf{Z}_t(\mathbf{q}_t, \dot{\mathbf{q}}_t)\dot{\mathbf{q}}_t - \mathbf{G}_t(\mathbf{q}_t) + \mathbf{l}_d) \tag{7}$$

where the symbol $\mathbf{M}(\mathbf{q}_t) \in \Re^{n \times n}$ represents the inertia matrix, which is always positive definite. $\mathbf{q}_t \in \Re^n$ denotes the position vector, while $\dot{\mathbf{q}}_t \in \Re^n$ and $\ddot{\mathbf{q}}_t \in \Re^n$ represent the velocity and acceleration vectors, respectively. $\boldsymbol{\tau} \in \Re^n$ stands for the actuator inputs applied to the system. The matrix $\mathbf{Z}_t(\mathbf{q}_t, \dot{\mathbf{q}}_t) \in \Re^{n \times n}$ encompasses centripetal and Coriolis forces. $\mathbf{G}_t(\mathbf{q}_t) \in \Re^n$ represents the gravity vector, and $\mathbf{l}_d \in \Re^n$ indicates the disturbance matrix.

Assume that the model parameters $\mathbf{M}(\mathbf{q}_t) = \mathbf{M}_0(\mathbf{q}_t) + \Delta\mathbf{M}(\mathbf{q}_t)$, $\mathbf{Z}_t(\mathbf{q}_t, \dot{\mathbf{q}}_t) = \mathbf{Z}_{t0}(\mathbf{q}_t, \dot{\mathbf{q}}_t) + \Delta\mathbf{Z}_t(\mathbf{q}_t, \dot{\mathbf{q}}_t)$, and $\mathbf{G}_t(\mathbf{q}_t) = \mathbf{G}_{t0}(\mathbf{q}_t) + \Delta\mathbf{G}_t(\mathbf{q}_t)$. $\mathbf{M}_0(\mathbf{q}_t)$, $\mathbf{Z}_{t0}(\mathbf{q}_t, \dot{\mathbf{q}}_t)$, and $\mathbf{G}_{t0}(\mathbf{q}_t)$ express the nominal values. $\Delta\mathbf{M}(\mathbf{q}_t), \Delta\mathbf{Z}_t(\mathbf{q}_t, \dot{\mathbf{q}}_t)$, and $\Delta\mathbf{G}_t(\mathbf{q}_t)$ express the unknown parts.

The dynamic model (7), can be further formulated in a form given below

$$\ddot{\mathbf{q}}_t = \mathbf{M}^{-1}(\mathbf{q}_t)\boldsymbol{\tau} + \mathbf{Q}(\mathbf{q}_t, \dot{\mathbf{q}}_t) + \mathbf{D}. \tag{8}$$

where $\mathbf{Q}(\mathbf{q}_t, \dot{\mathbf{q}}_t) = \mathbf{M}_0^{-1}(\mathbf{q}_t)(-\mathbf{Z}_{t0}(\mathbf{q}_t, \dot{\mathbf{q}}_t)\dot{\mathbf{q}}_t - \mathbf{G}_{t0}(\mathbf{q}_t))$ shows the known lumped component of the dynamics of EL system, and $\mathbf{D} = \mathbf{M}_0^{-1}(\mathbf{q}_t)(\mathbf{l}_d - \Delta\mathbf{M}(\mathbf{q}_t)\ddot{\mathbf{q}}_t - \Delta\mathbf{Z}_t(\mathbf{q}_t, \dot{\mathbf{q}}_t)\dot{\mathbf{q}}_t - \Delta\mathbf{G}_t(\mathbf{q}_t))$ is the lumped component of the EL system which is not known. The following shows equation (8) in state-space form: if we define the state variables to be $\mathbf{x}_1 = \mathbf{q}_t$ and $\mathbf{x}_2 = \dot{\mathbf{q}}_t$ respectively:

$$\begin{cases} \dot{\mathbf{x}}_1 = \mathbf{x}_2 \\ \dot{\mathbf{x}}_2 = \mathbf{M}_0^{-1}(\mathbf{x}_1)\boldsymbol{\tau} + \mathbf{Q}(\mathbf{x}_1, \mathbf{x}_2) + \mathbf{D} \end{cases}. \tag{9}$$

By using Eq. (9) and by defining trajectory tracking error as $\zeta_1 = \mathbf{x}_1 - \mathbf{q}_d$, and its derivative as $\zeta_2 = \mathbf{x}_2 - \dot{\mathbf{q}}_d$ in which $\mathbf{q}_d \in \Re^n$ denotes the desired trajectory and $\dot{\mathbf{q}}_d \in \Re^n$ its derivative respectively. The error equation of the EL system becomes:

$$\begin{cases} \dot{\zeta}_1 = \zeta_2 \\ \dot{\zeta}_2 = \mathbf{C}(\zeta)\mathbf{u} + \mathbf{H}(\zeta) + \mathbf{D} \end{cases} \tag{10}$$

with $\mathbf{C}(\zeta) = \mathbf{M}_0^{-1}(\mathbf{x}_1), \mathbf{H}(\zeta) = \mathbf{Q}(\mathbf{x}_1, \mathbf{x}_2) - \ddot{\mathbf{q}}_d, \mathbf{u} = \boldsymbol{\tau}$.

Assumption 1: It is assumed that the lumped uncertainty remains within certain bounds, where these bounds are defined by

$$\|\mathbf{D}\| \le b_0 + b_1\|\mathbf{q}_t\| + b_2\|\dot{\mathbf{q}}_t\|^2 \tag{11}$$

where b_0, b_1, and b_2 are positive constant.

3. MAIN RESULTS

In this section, the main aim is to bolster the trajectory tracking capabilities of an EL system despite uncertainties and external disturbances while ensuring swift convergence of the tracking error. Achieving this objective revolves around the development of an adaptive FTNSM control law. Furthermore, the fixed-time stability of the closed-loop system is rigorously validated and substantiated by theoretical underpinnings.

3.1 FTNSM surface design

To enhance convergence characteristics, the ensuing FTNSM variable is formulated as follows:

$$\boldsymbol{\sigma} = \zeta_2 + \chi(\zeta_1)\left(\boldsymbol{\alpha}_1 \mathbf{sig}(\zeta_1)^{\Theta} + \boldsymbol{\alpha}_2 \boldsymbol{\sigma}_d(\zeta_1)\right) \tag{12}$$

where $\boldsymbol{\sigma} = [\sigma_1, \sigma_2, ..., \sigma_n]^{\mathrm{T}} \in \Re^n$,

$\chi(\zeta_1) = 1 + 2\Lambda_a \arctan\left(\Lambda_b \|\zeta_1\|^{\Lambda_c}\right)/\pi$ with Λ_a, Λ_b and Λ_c denote adjustable positive values,

$\Theta = (1/2) + (\Theta_1/2\Theta_2) + ((\Theta_1/2\Theta_2) - (1/2))\operatorname{sign}(\|\zeta_1\| - 1)$

with Θ_1 and Θ_2 denote positive odd integers which satisfy

$\Theta_1 > \Theta_2$, $\boldsymbol{\alpha}_1 = \mathrm{diag}(\alpha_{11}, \alpha_{12}, ..., \alpha_{1n})$ and $\boldsymbol{\alpha}_2 = \mathrm{diag}(\alpha_{21}, \alpha_{22}, ..., \alpha_{2n})$ are positive diagonal matrices, $\boldsymbol{\sigma}_d(\boldsymbol{\zeta}_1) = [\sigma_{d1}, \sigma_{d2}, ..., \sigma_{dn}]^{\mathrm{T}} \in \Re^n$ with σ_{di} is defined as

$$\sigma_{di} = \begin{cases} \mathrm{sig}^{\frac{\Theta_3}{\Theta_4}}(\zeta_{1i}) \ \ if\ \bar{\sigma}_i = 0 \text{ or} (\bar{\sigma}_i \neq 0, |\zeta_{1i}| \geq \Delta_{\sigma i}) \\ j_{1i}\zeta_{1i} + j_{2i}\mathrm{sign}(\zeta_{1i})\zeta_{1i}^2 \ \ if\ \bar{\sigma}_i \neq 0, |\zeta_{1i}| < \Delta_{\sigma i} \end{cases} \tag{13}$$

where Θ_3 and Θ_4 denote positive odd integers which satisfy $\Theta_4 > \Theta_3$, and j_{1i} and j_{2i} are formulated in a form $j_{1i} = (2\Theta_4 - \Theta_3/\Theta_4)\Delta_{\sigma i}^{(\Theta_3/\Theta_4)-1}$, $j_{2i} = (\Theta_3 - \Theta_4/\Theta_4)\Delta_{\sigma i}^{(\Theta_3/\Theta_4)-2}$ to guarantee the continuity of the sliding mode variable (12). $\Delta_{\sigma i}$ represents a positive constant with value greater than zero. Furthermore, $\bar{\sigma}_i$ in the above (13) is used to show the ith element of $\bar{\boldsymbol{\sigma}}$, $i = 1, 2, ..., n$ and the $\bar{\boldsymbol{\sigma}}$ is stated as follows

$$\bar{\boldsymbol{\sigma}} = \boldsymbol{\zeta}_2 + \chi(\boldsymbol{\zeta}_1)\left(\boldsymbol{\alpha}_1 \mathbf{sig}(\boldsymbol{\zeta}_1)^{\Theta} + \boldsymbol{\alpha}_2 \mathbf{sig}(\boldsymbol{\zeta}_1)^{\frac{\Theta_3}{\Theta_4}}\right) \tag{14}$$

Theorem 1. Take into account the EL system described by equation (10), once its states reach the FTNSM surface, i.e., $\boldsymbol{\sigma} = \bar{\boldsymbol{\sigma}} = 0$, then $\boldsymbol{\zeta}_1 = 0$ and $\boldsymbol{\zeta}_2 = 0$ can be attained in fixed-time regardless of the initial values of the system states. The upper bound on convergence time is given by

$$T_\sigma \leq \max_{1\leq i\leq n}\left\{\frac{\Theta_4}{\alpha_{1i}(\Theta_4 - \Theta_3)}\ln\left(1 + \frac{\alpha_{1i}}{\alpha_{2i}}\right) + \frac{\Theta_2}{\alpha_{1i}(\Theta_1 - \Theta_2)}\right\} \tag{15}$$

Proof: Please refer to "Appendix A".

Remark 1. The function $\chi(\zeta_1)$ within FTNSM variable (12) plays a role in modulating the convergence rate, spanning from $1 + \Lambda_a$ to 1. As the states depart from the origin, $\chi(\zeta_1)$ tends towards $1 + \Lambda_a$, thereby amplifying the convergence rate. Conversely, when states approach the origin, $\chi(\zeta_1)$ converges to 1. This functionality enhances convergence by dynamically adapting to the proximity of the states. Furthermore, a new variable power term Θ is incorporated into FTNSM variable (12), adjusting according to the system's states. In close proximity to the origin, the nonlinear term $\mathrm{sig}^{\Theta_1/\Theta_2}(\zeta_1)$ is replaced by a linear term, resulting in a notable improvement in convergence. Thus, the proposed FTNSM variable exhibits superior convergence performance, whether the states are distant from or near the origin.

Remark 2. (Huang and Jia, 2017) introduced a fixed-time sliding variable represented as $\boldsymbol{\sigma} = \boldsymbol{\zeta}_2 + \boldsymbol{\alpha}_1 \mathbf{sig}(\boldsymbol{\zeta}_1)^{\Theta_1/\Theta_2} + \boldsymbol{\alpha}_2 \boldsymbol{\sigma}_d(\boldsymbol{\zeta}_1)$, with individual components given by $\bar{\sigma}_i = \zeta_{2i} + \alpha_{1i}\mathrm{sig}^{\Theta_1/\Theta_2}(\zeta_{1i}) + \alpha_{2i}\mathrm{sig}^{\Theta_3/\Theta_4}(\zeta_{1i})$. They derived the upper bound of convergence time as $T_a = \max_{1\leq i\leq n}\{(\Theta_4/\alpha_{2i}(\Theta_4 - \Theta_3)) + (\Theta_2/\alpha_{1i}(\Theta_1 - \Theta_2))\}$.

Another swiftly converging fixed-time sliding variable, $\sigma_i = \zeta_{2i} + \alpha_{1i}\zeta_{1i}^{(1/2)+(\Theta_1/2\Theta_2)+((\Theta_1/2\Theta_2)-(1/2))\mathrm{sign}(|\zeta_{1i}|-1)} + \alpha_2\zeta_{1i}^{\Theta_3/\Theta_4}$ was examined in (Ni et al., 2016), with its upper bound of convergence time is given by $T_b = \max_{1\leq i\leq n}\{(\Theta_4/\alpha_{2i}(\Theta_4 - \Theta_3)) \ln(1 + (\alpha_{1i}/\alpha_{2i})) + (\Theta_2/\alpha_{1i}(\Theta_1 - \Theta_2))\}$. As $\ln(1 + \alpha_{1i}/\alpha_{2i}) < \alpha_{1i}/\alpha_{2i}$ it follows that $T_\sigma < T_a$. Additionally, the development of the function $\chi(\zeta_1)$ leads to the observation that $T_\sigma < T_b$, indicating that under identical design parameters, the proposed FTNSM variable achieves the swiftest convergence rate.

3.2 Adaptive FTNSM control law design

Differentiating Equation (12) with respect to time and employing Equation (10), yields the following result.

$$\begin{aligned}\dot{\boldsymbol{\sigma}} = &\mathbf{C}(\boldsymbol{\zeta})\mathbf{u} + \mathbf{H}(\boldsymbol{\zeta}) + \mathbf{D} + \dot{\chi}(\boldsymbol{\zeta}_1)\left(\boldsymbol{\alpha}_1\mathbf{sig}(\boldsymbol{\zeta}_1)^{\Theta} + \boldsymbol{\alpha}_2\boldsymbol{\sigma}_d(\boldsymbol{\zeta}_1)\right) \\ &+ \chi(\boldsymbol{\zeta}_1)\left(\Theta\boldsymbol{\alpha}_1\mathrm{diag}\left(|\zeta_{1i}|^{\Theta-1}\right)\boldsymbol{\zeta}_2 + \boldsymbol{\alpha}_2\dot{\boldsymbol{\sigma}}_d(\boldsymbol{\zeta}_1)\right)\end{aligned} \tag{16}$$

where the ith component of vector $\dot{\boldsymbol{\sigma}}_d$ is expressed as follows:

$$\dot{\sigma}_{di} = \begin{cases} \frac{\Theta_3}{\Theta_4}|\zeta_{1i}|^{\frac{\Theta_3}{\Theta_4}-1}\zeta_{2i}, \ if\ \bar{\sigma}_i = 0 \text{ or} (\bar{\sigma}_i \neq 0, |\zeta_{1i}| \geq \Delta_{\sigma i}) \\ j_{1i}\zeta_{2i} + 2j_{2i}|\zeta_{1i}|\zeta_{2i}, \ if\ \bar{\sigma}_i \neq 0, |\zeta_{1i}| < \Delta_{\sigma i} \end{cases} \tag{17}$$

Under Assumption 1, it follows that

$$\begin{aligned}\|\mathbf{D}\| &\leq b_0 + b_1\|\mathbf{q}_t\| + b_2\|\dot{\mathbf{q}}_t\|^2 \\ &\leq h_1 + h_2 G\end{aligned} \tag{18}$$

where $h_1 = b_0$ and $h_2 = \max\{b_1, b_2\}$ are positive constant which are not known, $G = \|\mathbf{q}_t\| + \|\dot{\mathbf{q}}_{ti}\|^2$.

With the goal of achieving precise trajectory tracking, the subsequent adaptive FTNSM control law is formulated as

$$\mathbf{u} = \mathbf{u}_a + \mathbf{u}_b \tag{19}$$

where

$$\begin{aligned}\mathbf{u}_a = &-\mathbf{C}^{-1}(\boldsymbol{\zeta})\mathbf{H}(\boldsymbol{\zeta}) - \mathbf{C}^{-1}(\boldsymbol{\zeta})\dot{\chi}(\boldsymbol{\zeta}_1)\left(\boldsymbol{\alpha}_1\mathbf{sig}(\boldsymbol{\zeta}_1)^{\Theta} + \boldsymbol{\alpha}_2\boldsymbol{\sigma}_d(\boldsymbol{\zeta}_1)\right) \\ &- \mathbf{C}^{-1}(\boldsymbol{\zeta})\chi(\boldsymbol{\zeta}_1)\left(\Theta\boldsymbol{\alpha}_1\mathrm{diag}\left(|\zeta_{1i}|^{\Theta-1}\right)\boldsymbol{\zeta}_2 + \boldsymbol{\alpha}_2\dot{\boldsymbol{\sigma}}_d(\boldsymbol{\zeta}_1)\right)\end{aligned} \tag{20}$$

$$\begin{aligned}\mathbf{u}_b = &-\mathbf{C}^{-1}(\boldsymbol{\zeta})\Omega(\boldsymbol{\sigma})\left(\alpha_3\mathbf{sig}(\boldsymbol{\sigma})^{\phi} + \alpha_4\mathbf{sig}(\boldsymbol{\sigma})^{\varphi} + \alpha_5\boldsymbol{\sigma}\right) \\ &- \mathbf{C}^{-1}(\boldsymbol{\zeta})\mathbf{u}_v\end{aligned} \tag{21}$$

$$\Omega(\boldsymbol{\sigma}) = 1 + \Psi - \Psi\exp\left(-\nu\|\boldsymbol{\sigma}\|^{\mu}\right) \tag{22}$$

where $\phi = (1/2) + (\phi_1/2\phi_2) + ((\phi_1/2\phi_2) - (1/2))\mathrm{sign}(\|\boldsymbol{\sigma}\| - 1)$ with ϕ_1 and ϕ_2 denote positive odd integers which satisfy

$\phi_1 > \phi_2$, and $0 < \varphi < 1$. $\alpha_3, \alpha_4, \alpha_5, \Psi, \nu$ and μ denote positive values. $\mathbf{u}_v = [u_{v1}, u_{v2}, ..., u_{vn}]^T$ is used to represent the adaptive control component, defined as

$$u_{vi} = \begin{cases} \frac{\sigma_i}{|\sigma_i|}\left(\hat{h}_1 + \hat{h}_2 G\right), & |\sigma_i| \geq \Gamma, \\ \frac{\sigma_i}{\Gamma^2}\left(\hat{h}_1 + \hat{h}_2 G\right)^2, & |\sigma_i| < \Gamma, \end{cases} \quad i = 1, ..., n \tag{23}$$

Here, Γ stands for a small constant. The adaptation laws are then governed in the following manner:

$$\begin{aligned} \dot{\hat{h}}_1 &= \ell_1\left(\|\boldsymbol{\sigma}\| - \partial_1 \hat{h}_1\right), \\ \dot{\hat{h}}_2 &= \ell_2\left(\|\boldsymbol{\sigma}\| G - \partial_2 \hat{h}_2\right). \end{aligned} \tag{24}$$

Specifically, $\hat{h}_i$ $(i = 1, 2)$ denotes the estimated values of h_i. Additionally, $\ell_1, \ell_2, \partial_1$ and ∂_2 denote positive values.

Theorem 2. When applying the adaptive FTNSM control strategy outlined in (19) with the adaptive update laws in (24) to the EL system (10) under uncertainties and external disturbances, the closed-loop system attains practical fixed-time stability.

Proof. Please refer to "Appendix B".

Remark 3. One complexity of the proposed approach lies in tuning the control parameters $\Theta_i, \boldsymbol{\alpha}_1, \boldsymbol{\alpha}_2, \alpha_3, \alpha_4, \alpha_5, \phi_1, \phi_2, \varphi,$ $\ell_1, \ell_2, \partial_1$ and ∂_2, $i = 1, 2, 3, 4$ to achieve both high pointing accuracy and acceptable control effort. It is essential to consider the following guidelines when selecting these gains.

I. The settling time expressions show that the parameters $\Theta_i, \phi_1, \phi_2, \varphi$ have a significant impact on the system's convergence rate and accuracy.

II. Parameters j_{1i} and j_{2i} assure the continuity and differentiability of the function σ_{di}. When $\bar{\sigma}_i \neq 0$ and $|\zeta_{1i}| < \Delta_{\sigma i}$, the error states seamlessly shift from terminal sliding mode (TSM) to a general sliding manifold, thereby avoiding singularity issue in the case of $\bar{\sigma}_i \neq 0$ and $\zeta_{1i} = 0$. Additionally, by choosing a sufficiently small $\Delta_{\sigma i}$ that satisfies $|\zeta_{1i}| \geq \Delta_{\sigma i}$, as the sliding mode variable $\bar{\boldsymbol{\sigma}}$ approaches zero, the error ζ_{1i} will converge along $\bar{\boldsymbol{\sigma}}$. Consequently, the convergence of ζ_{1i} within a fixed-time can be guaranteed.

III. Increasing the values of $\boldsymbol{\alpha}_1, \boldsymbol{\alpha}_2, \alpha_3, \alpha_4, \alpha_5$ can improve convergence rates, but it may also result in larger overshoots and more control effort.

IV. The adaptive gains ℓ_1 and ℓ_2 influence the speeds at which uncertain parameters converge. These adaptive gains are usually chosen to be larger in order to attain a faster rate of convergence.

However, excessively large adaptive gains can negatively impact the performance of the control system.

V. To make the estimated bounds $\hat{h}_1$, and $\hat{h}_2$ closely follow the FTNSM surface, ∂_1 and ∂_2 are typically chosen to be small. However, excessively small values may reduce the convergence speed of these bounds. Thus, finding an optimal balance between the size of the bounded region and the convergence speed is crucial.

To obtain the necessary convergence rate and control precision, it is critical to choose these control gains correctly. However, there is no set technique for picking control gains; they are usually picked through trial and error until adequate control performance is attained. As a result, finding a tuning mechanism to alter control gains for optimal system performance is an important challenge and one of our future research goals. Figure 1 illustrates the structural block diagram of the proposed control mechanism while Figure 2 presents a flowchart outlining the control process.

4. ANALYSIS OF SIMULATION FINDINGS

In order to validate the effectiveness of the proposed adaptive FTNSM control algorithm, numerical simulations have been performed on a planar two-link manipulator in this section. The dynamic formulation for the two-link manipulator is delineated in reference (Boukattaya et al., 2018).

$$\mathbf{M}(\mathbf{q}_t) = \begin{bmatrix} m_{11} & m_{12} \\ m_{21} & m_{22} \end{bmatrix}, \mathbf{Z}_t(\mathbf{q}_t, \dot{\mathbf{q}}_t) = \begin{bmatrix} z_{11} & z_{12} \\ z_{21} & z_{22} \end{bmatrix}, \quad \mathbf{G}(\mathbf{q}_t) = [g_1 \quad g_2]^T \tag{25}$$

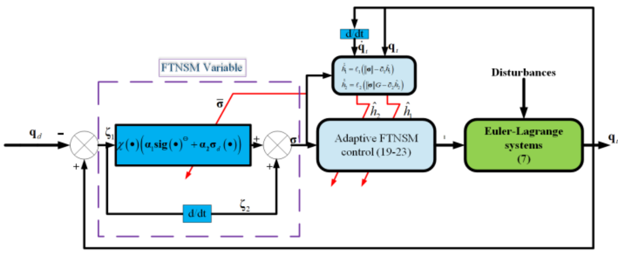

Fig. 1. Schematic illustration of the control system architecture.

where $\mathbf{q}_t = [q_{t1} \quad q_{t2}]^T$ represents the joint angle position vector of the joints, $m_{11} = (m_1 + m_2) l_1^2 + m_2 l_2^2 + 2 m_2 l_1 l_2 \cos(q_{t2}) + \bar{J}_1$, $m_{12} = m_{21} = m_2 l_2^2 + m_2 l_1 l_2 \cos(q_{t2})$, $m_{22} = m_2 l_2^2 + \bar{J}_2$, $z_{11} = -2 m_2 l_1 l_2 \sin(q_{t2}) \dot{q}_{t2}$, $z_{12} = -m_2 l_1 l_2 \sin(q_{t2}) \dot{q}_{t2}$, $z_{21} = m_2 l_1 l_2 \sin(q_{t2}) \dot{q}_{t1}$, $z_{22} = 0$, $g_1 = (m_1 + m_2) g l_1 \cos(q_{t1}) + m_2 g l_2 \cos(q_{t1} + q_{t2})$, $g_2 = m_2 g l_2 \cos(q_{t1} + q_{t2})$. l_1, l_2, m_1 and m_2 are the length and mass of the joints, $\bar{J}_1$ and $\bar{J}_2$ are the moment of inertia, g is the gravitational acceleration. The two link rigid robotic manipulator is depicted in Figure 3.

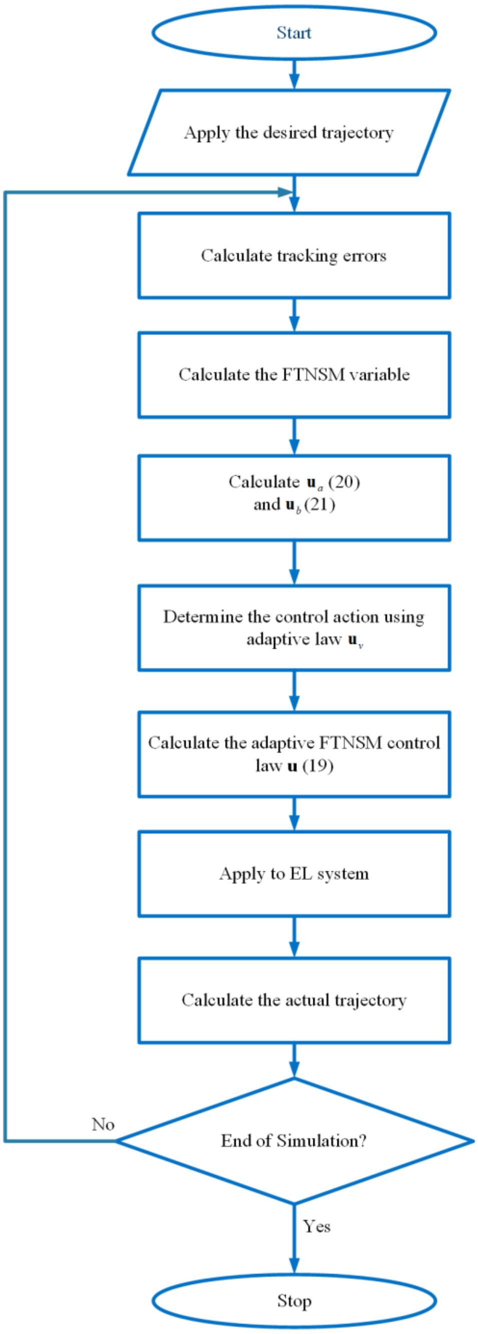

Fig. 2. The operational sequence of the proposed control system.

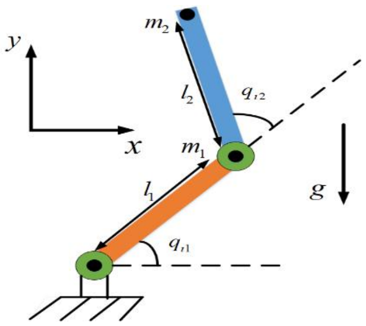

Fig. 3. Architecture of a two-link robotic manipulator.

The parameters values are selected as: $m_1 = 0.6\,\text{kg}, m_2 = 1.8\,\text{kg}, l_1 = 1\text{m}, l_2 = 0.8\text{m}, \bar{J}_1 = 6\,\text{kg.m}^2, \bar{J}_2 = 6\,\text{kg.m}^2$, and $g = 9.81\ \text{m/s}^2$. The nominal values of m_1 and m_2 are considered to be $m_{10} = 0.5\,\text{kg}$ and $m_{20} = 1.5\,\text{kg}$, respectively. Additionally, the nominal values of $\bar{J}_1$ and $\bar{J}_2$ are considered to be $\bar{J}_{10} = 5\,\text{kg.m}^2$ and $\bar{J}_{20} = 5\,\text{kg.m}^2$ respectively.

The representation of the disturbance term in the model is as follows:

$$\mathbf{l}_d = \begin{bmatrix} 2\sin(t) + 0.5\sin(200\pi t)(\mathbf{N}.\text{m}) \\ \cos(2t) + 0.5\sin(200\pi t)(\mathbf{N}.\text{m}) \end{bmatrix} \tag{26}$$

The system's desired trajectories are chosen as follows:

$$q_d = \begin{bmatrix} 0.2\cos(0.7t) + 0.2\cos(0.5t - 0.2)(\text{rad}) \\ 0.2\cos(0.5t - 0.2) - 0.2\cos(0.7t)(\text{rad}) \end{bmatrix} \tag{27}$$

The simulations utilized MATLAB/Simulink software with the Runge-Kutta solver and a time step of 1 millisecond (ms). The simulation experiments were conducted in two different scenarios. In the first, the proposed adaptive FTNSM was tested for its effectiveness in tracking the desired trajectory under uncertainties and disturbances. Its performance was compared to other state-of-the-art controllers, demonstrating its superiority in handling such challenges. The second scenario focused on evaluating the controller's performance for different initial state values. The parameters for the adaptive FTNSM controller are selected as: $\Lambda_a = 5, \Lambda_b = 2, \Lambda_c = 3, \Theta_1 = 9, \Theta_2 = 7, \Theta_3 = 11, \Theta_4 = 13, \boldsymbol{\alpha}_1 = \text{diag}(1.6, 1.7), \boldsymbol{\alpha}_2 = \text{diag}(0.7, 1.3), \Delta_{\sigma i} = 0.01, \phi_1 = 9, \phi_2 = 7, \varphi = 0.7, \Psi = 0.25, \nu = 4.5, \mu = 4, \alpha_3 = 0.9, \alpha_4 = 0.6, \alpha_5 = 0.6, \Gamma = 0.01, \ell_1 = \ell_2 = 1.4, \partial_1 = \partial_2 = 1.5$. By combining the results from Theorems 1 and 2, the settling time can be estimated as $T = \bar{T} + T_\sigma \approx 21s$.

4.1 Evaluation against alternative control methods

In this particular simulation scenario, the presumption is that the system is accommodating uncertainties and disturbances. To illustrate the improved effectiveness of the proposed adaptive FTNSM controller controller in the presence of uncertainties and diturbances, a comparative assessment is carried out against contemporary controllers aimed at enhancing the trajectory tracking performance of robot manipulators. These controllers include computed torque control (CTC) (Van et al., 2018) (Van et al., 2018) and Adaptive Nonsingular Fast Terminal Sliding-Mode Control (ANFTSMC) (Boukattaya et al., 2018). The design of CTC is outlined in (Van et al., 2018) with specified parameters $K_p = 200$ and $K_d = 20$ Additionally, ANFTSMC has been formulated according to the research conducted by (Boukattaya et al., 2018).

$$\sigma = \zeta_1 + \alpha_1 |\zeta_1|^{\alpha} \operatorname{sign}(\zeta_1) + \alpha_2 |\zeta_2|^{\beta} \operatorname{sign}(\zeta_2) \tag{28}$$

$$\begin{aligned} u = -C(\zeta_1)^{-1} \Big(& H_t(\zeta_1) + \frac{1}{\alpha_2 \beta} |\zeta_2|^{2-\beta} \left(1 + \alpha_1 \alpha |\zeta_1|^{\alpha-1}\right) \operatorname{sign}(\zeta_2) \\ & + k.\sigma + \left(\hat{b}_0 + \hat{b}_1 |q_t| + \hat{b}_2 |\dot{q}_t|^2 + \xi\right) \operatorname{sign}(\sigma) \Big) \end{aligned} \tag{29}$$

$$\begin{aligned} \dot{\hat{b}}_0 &= \lambda_0 |\sigma| |\zeta_2|^{\beta-1} \\ \dot{\hat{b}}_1 &= \lambda_1 |\sigma| |q_t| |\zeta_2|^{\beta-1} \\ \dot{\hat{b}}_2 &= \lambda_2 |\sigma| |\dot{q}_t|^2 |\zeta_2|^{\beta-1} \end{aligned} \tag{30}$$

The parameters of ANFTSMC are selected as follows: $\alpha = 2, \beta = 5/3, \xi = 0.5, \alpha_1 = \alpha_2 = 1, k = 50, \lambda_0 = \lambda_1 = \lambda_2 = 0.01$. The initial conditions for joint positions have been selected as $\mathbf{q}_t(0) = [0.5\text{rad}, 0.2\text{rad}]^{\mathrm{T}}$ and $\dot{\mathbf{q}}_t(0) = [0\text{rad/s}, 0\text{rad/s}]^{\mathrm{T}}$. σ denotes the NFTSM surface. For a clearer comparison, the position tracking performance and position tracking error for each joint of the manipulator robot are presented in Figures 4 and 5, respectively. Analysis of these figures reveals that the CTC exhibits inadequate tracking for the system. This deficiency is attributed to the challenges posed by uncertainties and disturbances, which the CTC fails to effectively manage within this system. Due to the robust nature of SMC in handling disturbances and uncertainties, the ANFTSMC demonstrates superior performance compared to the CTC, as evident in Figures 4 and 5.

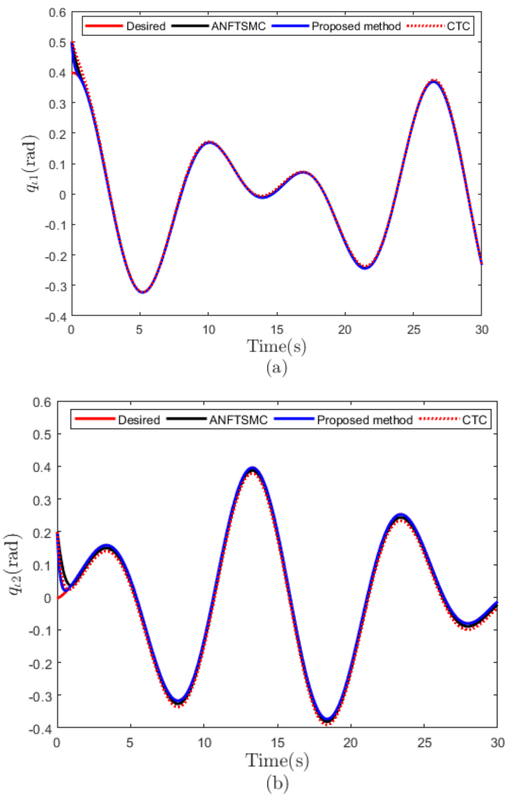

Fig. 4. Position tracking performance.

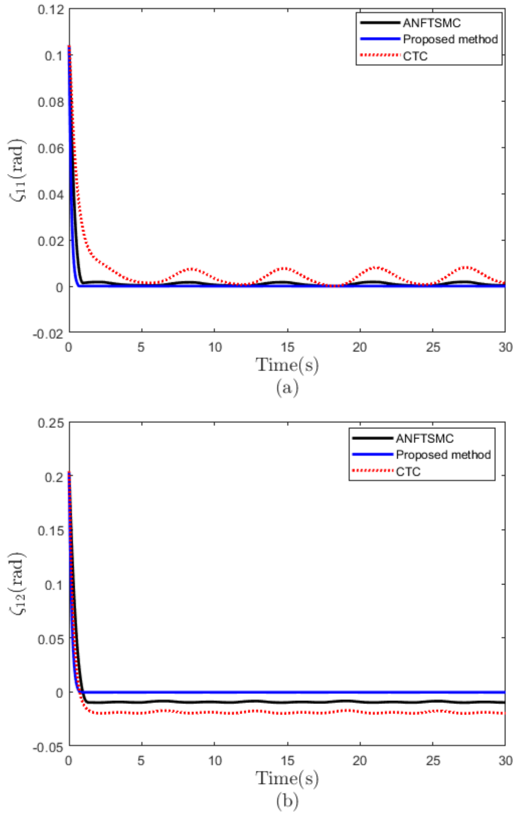

Fig. 5. Trajectory tracking errors, (a) at joint 1, (b) at joint 2.

Moreover, the proposed adaptive FTNSM controller surpasses both the CTC and ANFTSMC controllers in terms of position tracking and trajectory tracking error performance, as illustrated in Figures 3 and 4. However, the elapsed time in this study, representing the time MATLAB took to complete a 30-second simulation, was 1.50 seconds for CTC, 2.80 seconds for ANFTSMC, and 3.51 seconds for the proposed controller. Although the proposed method requires somewhat more computing time than CTC, the most basic control mechanism, the difference is not very significant. With today's improved hardware technology, the proposed technique can be implemented in real-world applications. Figures 6, 7, and 8 display the control inputs for the CTC, ANFTSMC, and adaptive FTNSM controller, respectively. Figure 8 illustrates that the proposed adaptive FTNSM control strategy effectively mitigated chattering. Similarly, the CTC exhibits smooth control input, as shown in Figure 6, due to the absence of the sign function in its design. While the ANFTSMC controller also generate continuous control input, as depicted in Figure 7, by utilizing $\tanh(x/\varepsilon), \varepsilon > 0$ instead of the sign function (Boukattaya et al., 2018), however this method, compromise system robustness and lead to increased steady-state error. Based on these findings, it can be concluded that the adaptive FTNSM control scheme outperforms both ANFTSMC and CTC schemes.

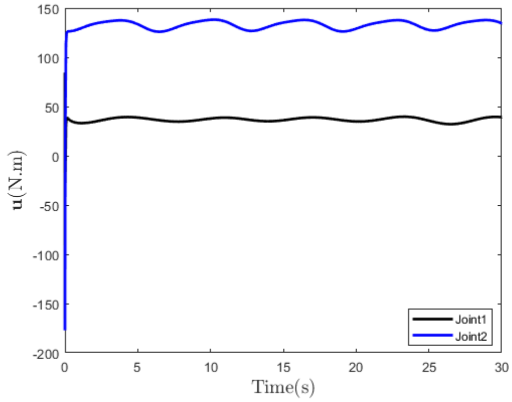

Fig. 6. Control input of the CTC controller.

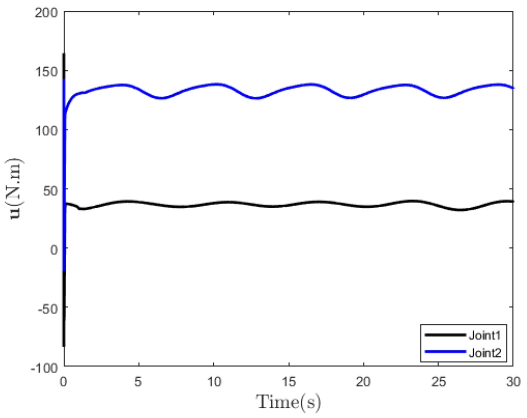

Fig. 7. Control input of the ANFTSMC controller.

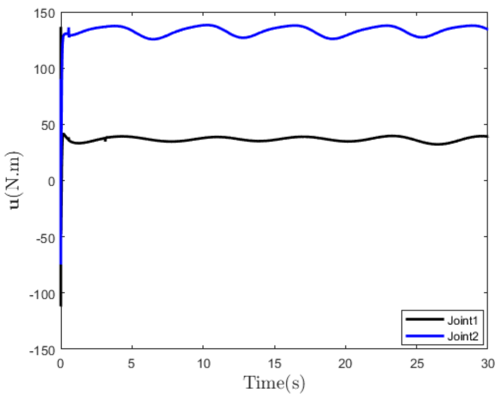

Fig. 8. Control input of the proposed controller.

4.2 Control performance across varying initial conditions

In this simulation, the effectiveness of the proposed control method for tracking the desired trajectory outlined in (27) is evaluated under system disturbances and uncertainties, with the assessment conducted across three distinct cases of initial state conditions as given in Table 1. The parameters for adaptive FTNSM control scheme are adjusted according to preceding analysis. Figure 9 depicts the results regarding position tracking, while Figure 10 illustrates the tracking error performance of the proposed controller across different initial conditions. Notably, the convergence times for different initial states are very similar, indicating a weak dependence on initial conditions. The total convergence time across all three cases is bounded by $2.3s$, which is in line with the analysis in Section 3. It confirms the study of the fixed-time characteristics reported in this paper and fully illustrates the efficacy of the fixed-time controller.

Table 1. Different initial values of the states.

Cases	Notations	Values
Case 1	$\mathbf{q}_t(0)$, $\dot{\mathbf{q}}_t(0)$	$[0.5, 0.2]^T$ rad , $[0,0]^T$ rad/s
Case 2		$[1, -0.5]^T$ rad , $[0,0]^T$ rad/s
Case3		$[-0.2, 0.6]^T$ rad ,$[0,0]^T$ rad/s

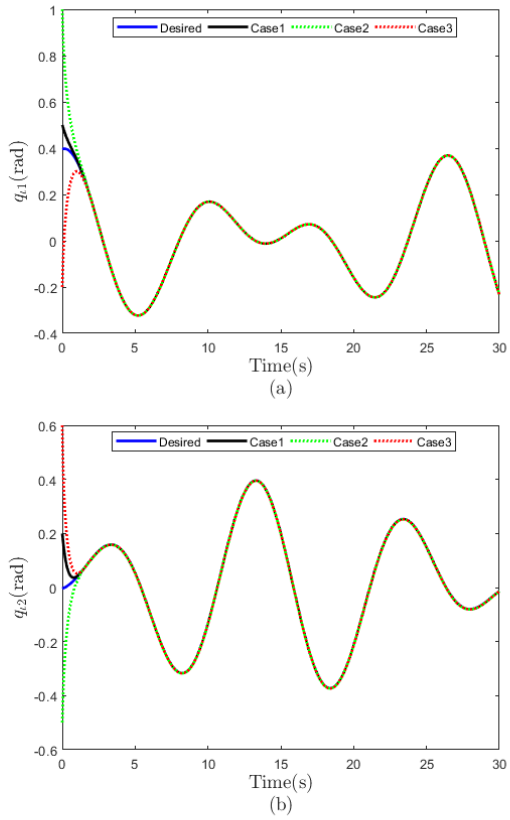

Fig. 9. Position tracking performance.

5. CONCLUSION

This work introduces a new adaptive control strategy for fixed-time trajectory tracking of a EL systems, even when facing system uncertainties, and external disturbances. To attain fixed-time control, it integrates adaptive techniques with a nonsingular fast terminal sliding variable based on the fixed-time method. The adaptive FTNSM controller developed, unlike existing fixed-time controls, avoids chattering and does not rely on information about lumped unknown component including uncertainties, and external disturbances. It also exhibits significantly faster convergence rate for system states, irrespective of their proximity to the origin, and as well as effectively addressing singularity issue. Through Lyapunov stability theory, it establishes explicit expressions for small convergence regions. Furthermore, the simulation analysis, considering uncertainties, and external disturbances, highlights the superior tracking performance of this designed control scheme among three different control approaches.

Future research will explore the impact of additional nonlinearities such as input saturation and measurement noise on system performance. Additionally, conducting practical

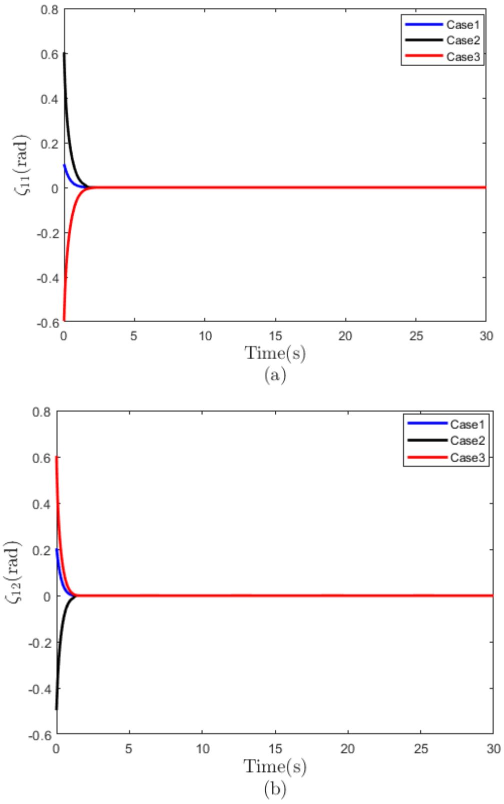

Fig. 10. Trajectory tracking errors, (a) at joint 1, (b) at joint 2.

experiments with the proposed control approach on real robot manipulator systems is an important avenue for further investigation.

ACKNOWLEDGEMENT

The authors would like to thank the Key Research and Development Program of Zhejiang Province, China, Grant/Award Number: 2022C03029; the funding of Leading Innovative and Entrepreneur Team Introduction Program of Zhejiang Province, Grant/Award Number: 2023R01006; Key Research and Development Program of Zhejiang Province, Grant/Award Number: 2024C03040; Science and Technology Innovation 2025 Major Project of Ningbo City, Grant/Award Number: 2023Z030 for their support in this research.

APPENDIX A (Proof of Theorem 1)

Upon reaching the FTNSM surface, that is, when $\boldsymbol{\sigma} = \bar{\boldsymbol{\sigma}} = 0$, a series of the ensuing differential equations can be derived as

$$\bar{\sigma}_i = \zeta_{2i} + \chi(\zeta_1)\left(\alpha_{1i}\mathrm{sig}^{\Theta}(\zeta_{1i}) + \alpha_{2i}\mathrm{sig}^{\frac{\Theta_3}{\Theta_4}}(\zeta_{1i})\right) = 0,\ i = 1,2,\ldots,n \tag{31}$$

By introducing a new state variable, denoted as P, defined as $P = |\zeta_{1i}|^{\Theta_4 - \Theta_3/\Theta_4}$ and utilizing equation (31), it consequently ensues that

$$\begin{aligned}\dot{P} &= -\frac{(\Theta_4-\Theta_3)\chi(\zeta_1)}{\Theta_4\mathrm{sig}^{\frac{\Theta_3}{\Theta_4}}(\zeta_{1i})}\left(\alpha_{1i}\mathrm{sig}^{\Theta}(\zeta_{1i}) + \alpha_{2i}\mathrm{sig}^{\frac{\Theta_3}{\Theta_4}}(\zeta_{1i})\right)\\ &= -\frac{(\Theta_4-\Theta_3)\chi(\zeta_1)}{\Theta_4}\left(\alpha_{1i}|\zeta_{1i}|^{-\frac{\Theta_3}{\Theta_4}+\Theta} + \alpha_{2i}\right)\\ &= -\frac{(\Theta_4-\Theta_3)\chi(\zeta_1)}{\Theta_4}\left(\alpha_{1i}P^{1+\frac{(\Theta-1)\Theta_4}{\Theta_4-\Theta_3}} + \alpha_{2i}\right)\end{aligned} \tag{32}$$

Regarding equation (31), the convergence time $T_{\sigma i}$ can be calculated through

$$\begin{aligned}T_{\sigma i} &= \frac{\Theta_4}{(\Theta_4-\Theta_3)}\int_0^{P(0)}\frac{1}{\chi(\zeta_1)\left(\alpha_{1i}P^{1+\frac{(\Theta-1)\Theta_4}{\Theta_4-\Theta_3}} + \alpha_{2i}\right)}dP\\ &= \frac{\Theta_4}{(\Theta_4-\Theta_3)}\int_0^{1}\frac{1}{\chi(\zeta_1)\left(\alpha_{1i}P^{1+\frac{(\Theta-1)\Theta_4}{\Theta_4-\Theta_3}} + \alpha_{2i}\right)}dP\\ &\quad+\frac{\Theta_4}{(\Theta_4-\Theta_3)}\int_1^{P(0)}\frac{1}{\chi(\zeta_1)\left(\alpha_{1i}P^{1+\frac{(\Theta-1)\Theta_4}{\Theta_4-\Theta_3}} + \alpha_{2i}\right)}dP\\ &= \frac{\Theta_4}{(\Theta_4-\Theta_3)}\int_0^{1}\frac{1}{\chi(\zeta_1)(\alpha_{1i}P + \alpha_{2i})}dP\\ &\quad+\frac{\Theta_4}{(\Theta_4-\Theta_3)}\int_1^{P(0)}\frac{1}{\chi(\zeta_1)(\alpha_{1i}P^{\Xi} + \alpha_{2i})}dP\end{aligned} \tag{33}$$

where $\Xi = 1 + ((\Theta_1-\Theta_2)\Theta_4)/((\Theta_4-\Theta_3)\Theta_2)$. As a result of the fact where $\chi(\zeta_1) \geq 1$, the convergence time $T_{\sigma i}$ is constrained by

$$\begin{aligned}T_{\sigma i} &\leq \frac{\Theta_4}{(\Theta_4-\Theta_3)}\left(\int_0^1\frac{1}{(\alpha_{1i}P+\alpha_{2i})}dP + \int_1^{P(0)}\frac{1}{(\alpha_{1i}P^{\Xi}+\alpha_{2i})}dP\right)\\ &< \frac{\Theta_4}{(\Theta_4-\Theta_3)}\left(\int_0^1\frac{1}{(\alpha_{1i}P+\alpha_{2i})}dP + \int_1^{P(0)}\frac{1}{(\alpha_{1i}P^{\Xi})}dP\right)\end{aligned} \tag{34}$$

with $\Xi > 1$, and $P(0) > 1$, $T_{\sigma i}$ is further bounded by

$$T_{\sigma i} \leq \frac{\Theta_4}{\alpha_{1i}(\Theta_4-\Theta_3)}\ln\left(1+\frac{\alpha_{1i}}{\alpha_{2i}}\right) + \frac{\Theta_2}{\alpha_{1i}(\Theta_1-\Theta_2)} \tag{35}$$

The above Equation (35) allows for the determination of the upper limit of the convergence time T_σ as follows

$$T_\sigma \le \max_{1\le i\le n}\left\{\frac{\Theta_4}{\alpha_{1i}(\Theta_4-\Theta_3)}\ln\left(1+\frac{\alpha_{1i}}{\alpha_{2i}}\right)+\frac{\Theta_2}{\alpha_{1i}(\Theta_1-\Theta_2)}\right\} \tag{36}$$

According to Equation (36), the maximum time required for convergence remains unaffected by the specific values of the system state. This implies that both error states ζ_1 and its derivative ζ_2 can reach the origin on the sliding surface within a fixed-time. This completes the proof.

APPENDIX B (Proof of Theorem 2)

The stability of the sliding phase and the reaching phase is separately examined through fixed-time analysis. Create a Lyapunov function in the form of

$$V_1=\frac{1}{2}\boldsymbol{\sigma}^T\boldsymbol{\sigma}+\frac{1}{2\ell_1}\tilde{h}_1^2+\frac{1}{2\ell_2}\tilde{h}_2^2 \tag{37}$$

where $\tilde{h}_1=h_1-\hat{h}_1$, $\tilde{h}_2=h_2-\hat{h}_2$. Upon calculating the time derivative of the aforementioned equation (37) and applying equations (16-23), the result is obtained as follows

$$\begin{aligned}\dot{V}_1&=\boldsymbol{\sigma}^T\dot{\boldsymbol{\sigma}}-\frac{1}{\ell_1}\tilde{h}_1\dot{\hat{h}}_1-\frac{1}{\ell_2}\tilde{h}_2\dot{\hat{h}}_2\\&=\boldsymbol{\sigma}^T\Big(\mathbf{C}(\zeta)\mathbf{u}+\mathbf{H}(\zeta)+\mathbf{D}+\dot{\chi}(\zeta_1)\big(\boldsymbol{\alpha}_1\mathbf{sig}(\zeta_1)^\Theta+\boldsymbol{\alpha}_2\boldsymbol{\sigma}_d(\zeta_1)\big)\\&\quad+\chi(\zeta_1)\big(\Theta\boldsymbol{\alpha}_1\mathrm{diag}(|\zeta_{1i}|^{\Theta-1})\zeta_2+\boldsymbol{\alpha}_2\dot{\boldsymbol{\sigma}}_d(\zeta_1)\big)\Big)-\sum_{i=1}^{2}\frac{1}{\ell_i}\tilde{h}_i\dot{\hat{h}}_i\\&\le-\Omega(\boldsymbol{\sigma})\boldsymbol{\sigma}^T\big(\alpha_3\mathbf{sig}(\boldsymbol{\sigma})^\phi+\alpha_4\mathbf{sig}(\boldsymbol{\sigma})^\varphi+\alpha_5\boldsymbol{\sigma}\big)-\boldsymbol{\sigma}^T\mathbf{u}_v\\&\quad+\|\boldsymbol{\sigma}\|\|\mathbf{D}\|-\sum_{i=1}^{2}\frac{1}{\ell_i}\tilde{h}_i\dot{\hat{h}}_i\end{aligned} \tag{38}$$

When $|\sigma_i|\ge\Gamma$, employing $\mathbf{u}_v$ and the adaption laws (24) into (38) produces

$$\begin{aligned}\dot{V}_1&\le-\Omega(\boldsymbol{\sigma})\boldsymbol{\sigma}^T\big(\alpha_3\mathbf{sig}(\boldsymbol{\sigma})^\phi+\alpha_4\mathbf{sig}(\boldsymbol{\sigma})^\varphi+\alpha_5\boldsymbol{\sigma}\big)-\|\boldsymbol{\sigma}\|\big(\hat{h}_1+\hat{h}_2G\big)\\&\quad+\|\boldsymbol{\sigma}\|(h_1+h_2G)-\tilde{h}_1\big(\|\boldsymbol{\sigma}\|-\partial_1\hat{h}_1\big)-\tilde{h}_2\big(\|\boldsymbol{\sigma}\|G-\partial_2\hat{h}_2\big)\\&\le-\Omega(\boldsymbol{\sigma})\boldsymbol{\sigma}^T\big(\alpha_3\mathbf{sig}(\boldsymbol{\sigma})^\phi+\alpha_4\mathbf{sig}(\boldsymbol{\sigma})^\varphi\big)+\partial_1\tilde{h}_1\hat{h}_1+\partial_2\tilde{h}_2\hat{h}_2.\end{aligned} \tag{39}$$

For any $l_i>1/2$ (where $i=1,2$), the subsequent inequalities remain valid.

$$\tilde{h}_i\dot{\hat{h}}_i\le-\frac{(2l_i-1)}{2l_i}\tilde{h}_i^2+\frac{l_i}{2}h_i^2 \tag{40}$$

By substituting (40) into (39), it follows that

$$\begin{aligned}\dot{V}_1&\le-\Omega(\boldsymbol{\sigma})\left(\alpha_3\sum_{i=1}^{n}|\sigma_i|^{\phi+1}+\alpha_4\sum_{i=1}^{n}|\sigma_i|^{\varphi+1}\right)\\&\quad-\big(\varpi_1\tilde{h}_1^2/2\ell_1\big)^{(\phi+1)/2}-\big(\varpi_1\tilde{h}_1^2/2\ell_1\big)^{(\varphi+1)/2}\\&\quad-\big(\varpi_2\tilde{h}_2^2/2\ell_2\big)^{(\phi+1)/2}-\big(\varpi_2\tilde{h}_2^2/2\ell_2\big)^{(\varphi+1)/2}\\&\quad+\kappa\end{aligned} \tag{41}$$

where

$$\begin{aligned}\kappa&=\big(\varpi_1\tilde{h}_1^2/2\ell_1\big)^{(\phi+1)/2}+\big(\varpi_1\tilde{h}_1^2/2\ell_1\big)^{(\varphi+1)/2}\\&\quad+\big(\varpi_2\tilde{h}_2^2/2\ell_2\big)^{(\phi+1)/2}+\big(\varpi_2\tilde{h}_2^2/2\ell_2\big)^{(\varphi+1)/2}\\&\quad+(\partial_1l_1/2)h_1^2+(\partial_2l_2/2)h_2^2-(\varpi_1/\ell_1)\tilde{h}_1^2\\&\quad-(\varpi_2/\ell_2)\tilde{h}_2^2\end{aligned} \tag{42}$$

with $\varpi_1=\ell_1\dfrac{\partial_1(2l_1-1)}{2l_1}$, and $\varpi_2=\ell_2\dfrac{\partial_2(2l_2-1)}{2l_2}$.

If $(\varpi_1/\ell_1)\tilde{h}_1^2\ge1$, it implies that

$$\begin{aligned}&\big(\vartheta_1\tilde{h}_1^2/2\ell_1\big)^{(\phi+1)/2}+\big(\vartheta_1\tilde{h}_1^2/2\ell_1\big)^{(\varphi+1)/2}-(\varpi_1/\ell_1)\tilde{h}_1^2\\&\le\big(\vartheta_1\tilde{h}_1^2/2\ell_1\big)^{(\phi+1)/2}-(\varpi_1/\ell_1)\tilde{h}_1^2.\end{aligned} \tag{43}$$

On the contrary, If $(\varpi_1/\ell_1)\tilde{h}_1^2<1$, it implies that

$$\begin{aligned}&\big(\vartheta_1\tilde{h}_1^2/2\ell_1\big)^{(\phi+1)/2}+\big(\vartheta_1\tilde{h}_1^2/2\ell_1\big)^{(\varphi+1)/2}-(\varpi_1/\ell_1)\tilde{h}_1^2\\&\le\big(\vartheta_1\tilde{h}_1^2/2\ell_1\big)^{(\varphi+1)/2}-(\varpi_1/\ell_1)\tilde{h}_1^2\le1.\end{aligned} \tag{44}$$

Given the existence of unknown constants $\bar{h}_1$ and $\bar{h}_2$, along with a compact set E defined as $E=f(\tilde{h}_1,\tilde{h}_2)$ such that $|\tilde{h}_1|\le\bar{h}_1$ and $|\tilde{h}_2|\le\bar{h}_2$, it follows that

$$\begin{aligned}&\big(\vartheta_1\tilde{h}_1^2/2\ell_1\big)^{(\phi+1)/2}+\big(\vartheta_1\tilde{h}_1^2/2\ell_1\big)^{(\varphi+1)/2}-(\varpi_1/\ell_1)\tilde{h}_1^2\\&\le\max\Big(\big(\vartheta_1\bar{h}_1^2/2\ell_1\big)^{(\phi+1)/2}-1,1\Big).\end{aligned} \tag{45}$$

Likewise, the inequalities are provided

$$\begin{aligned}&\big(\vartheta_2\tilde{h}_2^2/2\ell_2\big)^{(\phi+1)/2}+\big(\vartheta_2\tilde{h}_2^2/2\ell_2\big)^{(\varphi+1)/2}-(\varpi_2/\ell_2)\tilde{h}_2^2\\&\le\max\Big(\big(\vartheta_2\bar{h}_2^2/2\ell_2\big)^{(\phi+1)/2}-1,1\Big).\end{aligned} \tag{46}$$

Based on the aforementioned analyses and applying Lemma 2 and 3, (38) can be stated as follows

$$\dot{V}_1\le-\Pi_1V_1^{(\phi+1)/2}-\Pi_2V_1^{(\varphi+1)/2}+\amalg_1, \tag{47}$$

where $\Pi_1=3^{(1-\phi)/2}\min\big(2^{(1+\phi)/2}n^{(1-\phi)/2}\alpha_3,\varpi_i^{(1+\phi)/2}\big)$, $\Pi_2=\min\big(2^{(1+\varphi)/2}\alpha_4,\varpi_i^{(1+\varphi)/2}\big)$, and $\amalg_1=(\partial_1l_1/2)h_1^2+$

$\max\Big(\big(\vartheta_1\bar{h}_1^2/2\ell_1\big)^{(\phi+1)/2}-1,1\Big)+(\partial_2l_2/2)h_2^2+\max\Big(\big(\vartheta_2\bar{h}_2^2/2\ell_2\big)^{(\phi+1)/2}-1,1\Big).$

When $|\sigma_i|<\Gamma$, substituting (23) and (24) into (38) yields

$$\begin{aligned}\dot{V}_1&\le-\Omega(\boldsymbol{\sigma})\boldsymbol{\sigma}^T\big(\alpha_3\mathbf{sig}(\boldsymbol{\sigma})^\phi+\alpha_4\mathbf{sig}(\boldsymbol{\sigma})^\varphi\big)+\partial_1\tilde{h}_1\hat{h}_1+\partial_2\tilde{h}_2\hat{h}_2\\&\quad-\sum_{i=1}^{n}\left(\frac{|\sigma_i|}{\Gamma}\big(\hat{h}_1+\hat{h}_2G\big)-\frac{\Gamma}{2}\right)^2+\frac{n}{4}\Gamma^2.\end{aligned} \tag{48}$$

Using the identical analysis as in the scenario where $|\sigma_i| \geq \Gamma$, the above inequality can be stated as

$$\dot{V}_1 \leq -\Pi_1 V_1^{(\phi+1)/2} - \Pi_2 V_1^{(\varphi+1)/2} + \amalg_2 \quad (49)$$

with $\amalg_2 = \amalg_1 + n\Gamma^2/4$.

Hence, as per Lemma 1, the FTNSM variable (12) is stable and reaches a specific area Φ based on (49) in a finite time $\bar{T}$.

$$\Phi = \left\{ \lim_{t \to \bar{T}} \boldsymbol{\sigma} \,|\, \|\boldsymbol{\sigma}\| \leq \Phi_\sigma \right\} \quad (50)$$

$$\Phi_\sigma = \min\left\{ \left(\frac{\amalg_2}{(1-\upsilon_\theta)\Pi_1} \right)^{\frac{2}{\phi+1}}, \left(\frac{\amalg_2}{(1-\upsilon_\theta)\Pi_2} \right)^{\frac{2}{\varphi+1}} \right\} \quad (51)$$

$$\bar{T} \leq \left\{ \frac{2}{\Pi_1(1-\varphi)} \ln\left(1 + \frac{\Pi_1}{\Pi_2}\right) + \frac{2\phi_2}{\Pi_1(\phi_1 - \phi_2)} \right\} \quad (52)$$

where $0 < \upsilon_\theta < 1$.

Upon $\boldsymbol{\sigma}$ entering the specified region Φ, the system's fixed-time convergence property ought to be demonstrated in the ensuing analysis.

When the $\bar{\sigma}_i = 0$ condition is met, it is easily deduced from Theorem 1 that achieving tracking errors $\boldsymbol{\zeta}_1 = 0$ and $\boldsymbol{\zeta}_2 = 0$ occurs within a fixed timeframe.

When $\bar{\sigma}_i \neq 0$ and $|\zeta_{1i}| \geq \Delta_{\sigma i}$ we have

$$\bar{\sigma}_i = \zeta_{2i} + \chi(\boldsymbol{\zeta}_1)\left(\alpha_{1i}\mathrm{sig}^{\Theta}(\zeta_{1i}) + \alpha_{2i}\mathrm{sig}^{\frac{\Theta_3}{\Theta_4}}(\zeta_{1i}) \right) = \upsilon_{\sigma i}, \ |\upsilon_{\sigma i}| \leq \Phi \quad (53)$$

Subsequently, (53) can be expressed in an alternative manner as follows:

$$\begin{aligned} &\zeta_{2i} + \chi(\boldsymbol{\zeta}_1)\left(\alpha_{1i} - \frac{\upsilon_{\sigma i}}{\chi(\boldsymbol{\zeta}_1)|\zeta_{1i}|^{\Theta}\mathrm{sign}(\zeta_{1i})} \right)|\zeta_{1i}|^{\Theta}\mathrm{sign}(\zeta_{1i}) \\ &\quad + \chi(\boldsymbol{\zeta}_1)\alpha_{2i}|\zeta_{1i}|^{\frac{\Theta_3}{\Theta_4}}\mathrm{sign}(\zeta_{1i}) = 0, \end{aligned} \quad (54)$$

$$\begin{aligned} &\chi(\boldsymbol{\zeta}_1)\left(\alpha_{2i} - \frac{\upsilon_{\sigma i}}{\chi(\boldsymbol{\zeta}_1)|\zeta_{1i}|^{\frac{\Theta_3}{\Theta_4}}\mathrm{sign}(\zeta_{1i})} \right)|\zeta_{1i}|^{\frac{\Theta_3}{\Theta_4}}\mathrm{sign}(\zeta_{1i}) \\ &\quad + \zeta_{2i} + \chi(\boldsymbol{\zeta}_1)\alpha_{1i}|\zeta_{1i}|^{\Theta}\mathrm{sign}(\zeta_{1i}) = 0, \end{aligned} \quad (55)$$

As per the expression given in Eq. (54),and Eq. (55), when the $\alpha_{1i} - \left(\upsilon_{\sigma i}/\chi(\boldsymbol{\zeta}_1)|\zeta_{1i}|^{\Theta}\mathrm{sign}(\zeta_{1i})\right) > 0$, and $\alpha_{2i} - \left(\upsilon_{\sigma i}/\chi(\boldsymbol{\zeta}_1)|\zeta_{1i}|^{\frac{\Theta_3}{\Theta_4}}\mathrm{sign}(\zeta_{1i})\right) > 0$ hold true, Eq. (54),and Eq. (55) preserve the structure of the FTNSM variable (12), and the system states can achieve convergence at a fixed-time to regions such as $|\zeta_{1i}| \leq \Phi_{\zeta_{1i}}$ and $|\zeta_{2i}| \leq \Phi_{\zeta_{2i}}$.

If $\bar{\sigma}_i \neq 0, |\zeta_{1i}| < \Delta_{\sigma i}$, given that the state $\boldsymbol{\zeta}_1$ has reached the region $\Phi_{\zeta_{1i}}$ in accordance with the (12), one can derive:

$$\begin{aligned} \bar{\sigma}_i = \zeta_{2i} + \chi(\boldsymbol{\zeta}_1)\big(&\alpha_{1i}\mathrm{sig}^{\Theta}(\zeta_{1i}) + \alpha_{2i}\left(j_{1i}\zeta_{1i} \right. \\ &\left. + j_{2i}\mathrm{sign}(\zeta_{1i})\zeta_{1i}^2 \right)\big) \end{aligned} \quad (56)$$

After time $\bar{T}$, the ensuing inequality can be derived.

$$\begin{aligned} |\zeta_{2i}| = |\bar{\sigma}_i| + \chi(\boldsymbol{\zeta}_1)\big(&\alpha_{1i}|\zeta_{1i}|^{\Theta} \\ &+ \alpha_{2i}\left| j_{1i}\zeta_{1i} + j_{2i}\mathrm{sign}(\zeta_{1i})\zeta_{1i}^2 \right|\big) \leq \Phi_{\zeta_{2i}} \end{aligned} \quad (57)$$

The preceding analysis demonstrates that the system states $\boldsymbol{\zeta}_1$ and $\boldsymbol{\zeta}_2$ will ultimately reach the area where $|\zeta_{1i}| \leq \Phi_{\zeta_{1i}}$ and $|\zeta_{2i}| \leq \Phi_{\zeta_{2i}}$ respectively, in a predetermined time period. Thus, the closed-loop system demonstrates practical fixed-time stability, completing the proof.

REFERENCES

Boukattaya M, Mezghani N and Damak T (2018) Adaptive nonsingular fast terminal sliding-mode control for the tracking problem of uncertain dynamical systems. *ISA transactions* 77: 1-19.

Cao L, Xiao B, Golestani M, et al. (2019) Faster fixed-time control of flexible spacecraft attitude stabilization. *IEEE Transactions on Industrial Informatics* 16(2): 1281-1290.

Chen Q, Xie S, Sun M, et al. (2018) Adaptive nonsingular fixed-time attitude stabilization of uncertain spacecraft. *IEEE Transactions on Aerospace and Electronic Systems* 54(6): 2937-2950.

Deng C, Wen C, Huang J, et al. (2021) Distributed observer-based cooperative control approach for uncertain nonlinear MASs under event-triggered communication. *IEEE transactions on Automatic Control* 67(5): 2669-2676.

Fallaha CJ, Saad M, Kanaan HY, et al. (2010) Sliding-mode robot control with exponential reaching law. *IEEE Transactions on Industrial Electronics* 58(2): 600-610.

Feng Y, Yu X and Man Z (2002) Non-singular terminal sliding mode control of rigid manipulators. *Automatica* 38(12): 2159-2167.

Gao J, Fu Z and Zhang S (2018) Adaptive fixed-time attitude tracking control for rigid spacecraft with actuator faults. *IEEE Transactions on Industrial Electronics* 66(9): 7141-7149.

Huang Y and Jia Y (2017) Adaptive fixed-time relative position tracking and attitude synchronization control for non-cooperative target spacecraft fly-around mission. *Journal of the Franklin Institute* 354(18): 8461-8489.

Huang Y and Jia Y (2018) Adaptive fixed-time six-DOF tracking control for noncooperative spacecraft fly-around mission. *IEEE Transactions on Control Systems Technology* 27(4): 1796-1804.

Jiang B, Hu Q and Friswell MI (2016) Fixed-time attitude control for rigid spacecraft with actuator saturation and faults. *IEEE Transactions on Control Systems Technology* 24(5): 1892-1898.

Jin X, Wang S, Qin J, et al. (2017) Adaptive fault-tolerant consensus for a class of uncertain nonlinear second-order multi-agent systems with circuit implementation. *IEEE Transactions on Circuits and Systems I: Regular Papers* 65(7): 2243-2255.

Mozayan SM, Saad M, Vahedi H, et al. (2016) Sliding mode control of PMSG wind turbine based on enhanced exponential reaching law. *IEEE Transactions on Industrial Electronics* 63(10): 6148-6159.

Ni J, Liu L, Liu C, et al. (2016) Fast fixed-time nonsingular terminal sliding mode control and its application to chaos suppression in power system. *IEEE Transactions on Circuits and Systems II: Express Briefs* 64(2): 151-155.

Polyakov A (2011) Nonlinear feedback design for fixed-time stabilization of linear control systems. *IEEE transactions on Automatic Control* 57(8): 2106-2110.

Qin J, Gao H and Zheng WX (2014) Exponential synchronization of complex networks of linear systems and nonlinear oscillators: A unified analysis. *IEEE transactions on neural networks and learning systems* 26(3): 510-521.

Ren C, Li X, Yang X, et al. (2019) Extended state observer-based sliding mode control of an omnidirectional mobile robot with friction compensation. *IEEE Transactions on Industrial Electronics* 66(12): 9480-9489.

Rezaei E, Bolandi H and Fathi M (2024) Designing a fixed-time observer-based adaptive non-singular sliding mode controller for flexible spacecraft. *ISA transactions* 148: 32-44.

Saeed T, Abbas I and Marin M (2020) A GL model on thermo-elastic interaction in a poroelastic material using finite element method. *Symmetry* 12(3): 488.

Shtessel Y, Edwards C, Fridman L, et al. (2014) *Sliding mode control and observation.* Springer.

Song S, Park JH, Zhang B, et al. (2020) Event-triggered adaptive practical fixed-time trajectory tracking control for unmanned surface vehicle. *IEEE Transactions on Circuits and Systems II: Express Briefs* 68(1): 436-440.

Spong MW and Vidyasagar M (2008) *Robot dynamics and control.* John Wiley & Sons.

Sun Z, Xia Y, Dai L, et al. (2017) Disturbance rejection MPC for tracking of wheeled mobile robot. *IEEE/ASME Transactions on Mechatronics* 22(6): 2576-2587.

Tao M, Chen Q, He X, et al. (2019) Adaptive fixed-time fault-tolerant control for rigid spacecraft using a double power reaching law. *International Journal of Robust and Nonlinear Control* 29(12): 4022-4040.

Tian B, Zuo Z, Yan X, et al. (2017) A fixed-time output feedback control scheme for double integrator systems. *Automatica* 80: 17-24.

Van M, Mavrovouniotis M and Ge SS (2018) An adaptive backstepping nonsingular fast terminal sliding mode control for robust fault tolerant control of robot manipulators. *IEEE Transactions on Systems, Man, and Cybernetics: Systems* 49(7): 1448-1458.

Venkataraman S and Gulati S (1993) Control of nonlinear systems using terminal sliding modes.

Wang J, Yang Y, Xia J, et al. (2021) Coding-decoding-based sliding mode control for networked persistent dwell-time switched systems. *International Journal of Robust and Nonlinear Control* 31(12): 6055-6068.

Wang L, Chai T and Zhai L (2009) Neural-network-based terminal sliding-mode control of robotic manipulators including actuator dynamics. *IEEE Transactions on Industrial Electronics* 56(9): 3296-3304.

Zhang L, Liu H, Tang D, et al. (2021) Adaptive fixed-time fault-tolerant tracking control and its application for robot manipulators. *IEEE Transactions on Industrial Electronics* 69(3): 2956-2966.

Zuo Z (2015) Non-singular fixed-time terminal sliding mode control of non-linear systems. *IET Control Theory & Applications* 9(4): 545-552.

Zuo Z, Tian B, Defoort M, et al. (2017) Fixed-time consensus tracking for multiagent systems with high-order integrator dynamics. *IEEE transactions on Automatic Control* 63(2): 563-570.